Sensorless Force Approximation Control of 3-DOF Passive Haptic Devices

Maciej Łącki[1(✉)] and Carlos Rossa[2]

[1] Haply Robotics, Montreal, QC, Canada
maciej@haply.co
[2] Carleton University, Ottawa, ON, Canada
rossa@sce.carleton.ca

Abstract. Haptic devices using passive actuators such as brakes are intrinsically stable and offer greater transparency compared to traditional haptic devices actuated by electric motors. However, force control in passive haptic devices is particularly challenging and relies heavily on the use of force sensors, which can significantly increase the device's inertia and bandwidth. This paper proposes to use a nonlinear disturbance observer based on a Newtonian dynamic model of a 3-Degree-of-Freedom delta passive haptic device to estimate the force input of the user. The observer is tested using a series of simulations and the results confirm that the estimated input force closely matches the actual input force even when the system is subjected to unmodelled dynamics such as the brake's hysteresis.

Keywords: Force-feedback · Passive actuators · Force estimation

1 Introduction

Passive haptic devices offer unparalleled stability compared to traditional haptic devices actuated by electric motors. Their main limitation, however, is that multi-degree-of-freedom (DOF) passive haptic devices cannot generate forces in arbitrary directions. In fact, as discussed in [14], the portion of the workspace where forces can be displayed in any direction decreases rapidly with the number of degrees of freedom. To render forces outside of these regions, force approximation controllers need to be used. These control schemes typically attempt to eliminate the net force acting on the end-effector, perpendicular to the virtual surface, thereby ensuring that the device's end effector slides along the surface without penetrating it [3,15]. To balance the force at the end-effector these controllers require an accurate measurement of the user force input, which is typically achieved using a force sensor.

Force sensors are challenging to integrate in haptic devices as the added mass reduces transparency and measurement noise narrows the bandwidth [10]. An alternative to direct force sensing is to modify the force approximation scheme such that it considers the energy exchange between the virtual environment and the haptic device, eliminating the need for force measurement so long as the device moves [4]. However, in a stationary passive haptic device, the energy flow

S. Berretti and G.-M. Su (Eds.): ICSM 2022, LNCS 13497, pp. 381–394, 2022.
https://doi.org/10.1007/978-3-031-22061-6_28

is not observable and the direction of the user's force needs to be determined to control the device. This non-model-based controller is simple to integrate, however, it is difficult to adapt in multi-DOF. Thus, to void the use of a force sensor completely, the force input must be estimated.

Force estimation schemes generally use model-based disturbance observers to estimate an external force. In [11,12], the disturbance observer uses an inverse dynamic model with a low-pass filter to estimate the disturbances acting on the device. Expanding this observer to each joint of a multi-DOF manipulator allows for the estimation of the torque applied to each joint [18]. The observers presented in [11,12,18] base their structure on linearized models of highly nonlinear dynamics, which means that their stability is not guaranteed.

Nonlinear disturbance observers (NDOs) are a superior choice for robotic manipulators as they require no model linearization, no acceleration measurement, and are proven to be asymptotically stable. The first NDOs, introduced in [2], were limited to 2-DOF planar devices, however, their use quickly expanded to devices functioning in 3D space [13] followed by n-DOF manipulators in [19]. NDOs were previously used in haptic applications for closed-loop force [7] or impedance control [6] and in many other applications [17]. To the best of our knowledge, NDOs have not been used to estimate the input force in a multi-DOF haptic device.

This paper explores the possibility of using an NDO to estimate the force input in a passive haptic device. The preliminary analysis is based on the 3-DOF parallel device introduced in [15] and aims to prove, using simulations, that the force applied to a moving end-effector can be estimated, and that such an estimate is sufficient for force approximation control of the device.

To this end, Sect. 2 introduces the structure of the NDO, along with the dynamic model of the 3-DOF parallel passive device presented in [15]. Next, in Sect. 3 the observer is validated using a series of simulations aimed at proving the observer's ability to estimate various types of force inputs. The preliminary results are then evaluated in Sect. 4 to determine the feasibility of the presented approach in the context of controlling a multi-DOF passive haptic device without an accurate force measurement.

2 Force Observer Design

The NDO is model-based and thus it requires a dynamic model of the device. The device used to derive such a dynamic model is a 3-DOF haptic device with a modified Delta mechanism presented in [21].

2.1 Dynamic Model

The device we are considering uses particle brakes as actuators and employs a modified Delta kinematic structure as described in [21]. Let the position of each of the three actuated joints be $\boldsymbol{\theta} = [\theta_{11}\ \theta_{12}\ \theta_{13}]^{\mathrm{T}}$, the velocity be $d\boldsymbol{\theta}/dt = \ddot{\boldsymbol{\theta}}$

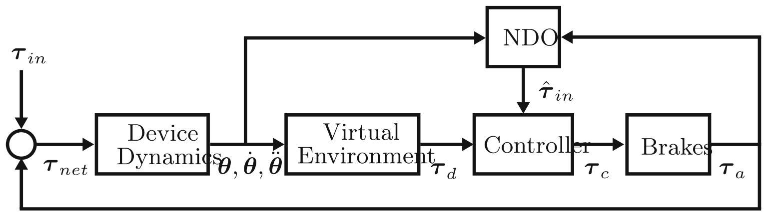

Fig. 1. The torque input estimate $\hat{\boldsymbol{\tau}}_{in}$ of the NDO replaces the torque measurement $\boldsymbol{\tau}_{in}$ as the input to the controller. The NDO requires measurements of the joint positions $\boldsymbol{\theta}$ and velocities $\dot{\boldsymbol{\theta}}$, along with the plant output estimate $\boldsymbol{\tau}_a$.

and acceleration be $d\dot{\boldsymbol{\theta}}/dt = \ddot{\boldsymbol{\theta}}$. Its dynamic model is given by the second order differential equation (Fig. 1)

$$\mathbf{M}(\boldsymbol{\theta})\ddot{\boldsymbol{\theta}} + \mathbf{C}(\boldsymbol{\theta}, \dot{\boldsymbol{\theta}})\dot{\boldsymbol{\theta}} + \mathbf{G}(\boldsymbol{\theta}) = \boldsymbol{\tau}_a + \boldsymbol{\tau}_{in} \tag{1}$$

where $\{\boldsymbol{\tau}_a, \boldsymbol{\tau}_{in}, \mathbf{G}(\boldsymbol{\theta})\} \in \mathbb{R}^{3\times 1}$, $\{\mathbf{M}(\boldsymbol{\theta}), \mathbf{C}(\boldsymbol{\theta}, \dot{\boldsymbol{\theta}})\} \in \mathbb{R}^{3\times 3}$ represent the applied torque, the input torque, the gravity vector, and the inertia and Coriolis matrices, respectively. The matrices in (1) are given using Newtonian dynamic analysis [21] as:

$$\begin{aligned}
\mathbf{M}(\boldsymbol{\theta}) &= I_a\mathbf{I} + m(\mathbf{J}^{-1})^{\mathrm{T}}\ \mathbf{J}^{-1} \\
\mathbf{C}(\boldsymbol{\theta}, \dot{\boldsymbol{\theta}}) &= c_d\mathbf{I} + m(\mathbf{J}^{-1})^{\mathrm{T}}\ \frac{d}{dt}(\mathbf{J}^{-1}) \\
\mathbf{G}(\boldsymbol{\theta}) &= -ag\left(\frac{m_a}{2} + m_b\right)\cos(\boldsymbol{\theta}) - m(\mathbf{J}^{-1})^{\mathrm{T}}\begin{bmatrix}0\\0\\g\end{bmatrix}
\end{aligned}$$

where $\mathbf{J} \in \mathbb{R}^{3\times 3}$ is the Jacobian matrix and

$$\begin{aligned}
I_a &= I_m + \frac{m_a a^2}{3} + m_b\ a^2 \\
m &= 3m_b + m_c
\end{aligned}$$

where m_a, m_b, and m_c, represent the mass of links a, b, and the end-effector; c_d is the viscous damping of the brake and g is the acceleration due to gravity. Note that there is no known closed form solution to $d/dt\ (\mathbf{J}^{-1})$ therefore this term must be approximated numerically [9]. The link lengths of the device are given in Table 1 while Table 2 summarizes their physical characteristics.

2.2 Nonlinear Disturbance Observer

The nonlinear disturbance observer, shown as a block diagram in Fig. 2, has the following form:

$$\dot{\mathbf{z}} = -\mathbf{L}(\boldsymbol{\theta}, \dot{\boldsymbol{\theta}})\mathbf{z} + \mathbf{L}(\boldsymbol{\theta}, \dot{\boldsymbol{\theta}})\left(\mathbf{C}(\boldsymbol{\theta}, \dot{\boldsymbol{\theta}}) + \mathbf{G}(\boldsymbol{\theta}) - \boldsymbol{\tau}_a - \mathbf{p}(\boldsymbol{\theta}, \dot{\boldsymbol{\theta}})\right) \tag{2a}$$

$$\hat{\boldsymbol{\tau}}_d = \mathbf{z} + \mathbf{p}(\boldsymbol{\theta}, \dot{\boldsymbol{\theta}}) \tag{2b}$$

Table 1. Links (top row) of the haptic device and their corresponding lengths in millimetres (bottom row) of the 3-DOF passive haptic device from [15]

Link Lengths in millimeters								
a	b	c	d	e	f	g	r	s
60.0	102.5	14.4	13.0	13.0	25.0	27.9	36.6	27.2

Table 2. Physical characteristics of each link in the 3-DOF passive haptic device. I_m is the brakes' mass moment of inertia, c_d is the viscous damping of the actuator, m_a the mass of link a, m_b is the equivalent mass of link b, and m_c is the mass of the end-effector.

I_m (mm^4)	m_a (g)	m_b (g)	m_c (g)	c_d (Ns/m)
8.5	6.8	16	10	0.01

where $\mathbf{z} \in \mathbb{R}^{3\times1}$ represents internal observer states, $\mathbf{L}(\boldsymbol{\theta}, \dot{\boldsymbol{\theta}}) \in \mathbb{R}^{3\times3}$ is the observer gain matrix given as,

$$\mathbf{L}(\boldsymbol{\theta}, \dot{\boldsymbol{\theta}})\ \mathbf{M}(\boldsymbol{\theta})\ddot{\boldsymbol{\theta}} = \left[\frac{\partial \mathbf{p}(\boldsymbol{\theta}, \dot{\boldsymbol{\theta}})}{\partial \boldsymbol{\theta}}\ \frac{\partial \mathbf{p}(\boldsymbol{\theta}, \dot{\boldsymbol{\theta}})}{\partial \dot{\boldsymbol{\theta}}}\right] \begin{bmatrix} \dot{\boldsymbol{\theta}} \\ \ddot{\boldsymbol{\theta}} \end{bmatrix} \tag{3}$$

and the auxiliary function $\mathbf{p}(\boldsymbol{\theta}, \dot{\boldsymbol{\theta}})$ which is used to substitute acceleration measurements [2]. For a 3-DOF manipulator a possible formulation for the auxiliary variable is [6]

$$\mathbf{p}(\boldsymbol{\theta}, \dot{\boldsymbol{\theta}}) = c \begin{bmatrix} \dot{\theta}_{11} \\ \dot{\theta}_{11} + \dot{\theta}_{12} \\ \dot{\theta}_{11} + \dot{\theta}_{12} + \dot{\theta}_{13} \end{bmatrix} \tag{4}$$

giving the observer gain matrix as

$$\mathbf{L}(\boldsymbol{\theta}, \dot{\boldsymbol{\theta}}) = c \begin{bmatrix} 1 & 0 & 0 \\ 1 & 1 & 0 \\ 1 & 1 & 1 \end{bmatrix} \mathbf{M}(\boldsymbol{\theta})^{-1} \tag{5}$$

which can be proven to be asymptotically stable for a range of c, which represents a controllable observer gain [2,13].

NDOs are formulated on assumptions that disturbance varies relatively slowly and that all functions in the dynamic model of the device are smooth. As shown in [2], however, NDOs can estimate fast varying disturbances. In the context of passive haptic devices, it must also be assumed that no brake is stationary during the operation, as the states of a stationary brake are not observable.

3 Simulation Results

Since a human operator can apply a wide range of forces to the device at a wide range of frequencies, the simulations must test the ability of the observer to

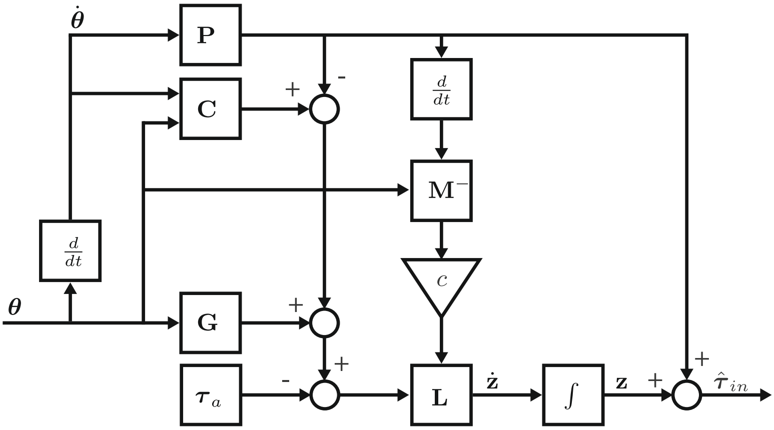

Fig. 2. The nonlinear disturbance observer estimates torque input $\hat{\boldsymbol{\tau}}_{in}$ using angular position $\boldsymbol{\theta}$, velocity $\dot{\boldsymbol{\theta}}$, and the torque applied by the brakes $\boldsymbol{\tau}_a$

estimate the input force in a variety of conditions. The testing scenarios 1 and 2, detailed below, validate the observer for cases where the device is not rendering forces to the user i.e., free motion. Scenarios 3 and 4, on the other hand, test the observer as the force sensing component in the force approximation scheme from [15]. Finally, scenarios 5 and 6 compare the observer and the controller performance with uncompensated brake hysteresis in the dynamic model of the device.

Scenario 1 - Free motion with constant vertical force input: In this scenario, the force applied to the end-effector has only a vertical Z component following a square wave pattern of ±400mN at a frequency of 1Hz. This scenario tests the NDO's ability to converge when subjected to an unsmooth force input.

Scenario 2 - Free motion with varying force input: The force simulates the user's input; it is smooth and varies in the X, Y, and Z axes. The magnitude of the applied forces in the Z axis is approximately 10N and 5N along the X and Y axes with a frequency of 3.5Hz. This scenario evaluates the observer's ability to estimate fast varying forces acting in arbitrary directions.

Scenario 3 - Rendering a displayable desired force in the vertical axis: Similar to the first scenario, the force input is a square wave in the Z axis with a magnitude of 400mN and a frequency of 2Hz, but the device attempts to render a force. The desired force is a sine wave with a magnitude of 100mN and a frequency of 1Hz. This scenario compares the output of the force approximation controller from [15] when using the actual and estimated force input.

Scenario 4 - Rendering partially displayable forces, with a varying force input: Like in Scenario 2 the force input simulates the user moving the device in the X, Y, axes and Z axes with a force magnitude of 10N in the Z axis, and 5N in the X and Y, all at a frequency of 3.5Hz. The desired force has a magnitude of 5N in the Z axis, and 2N in the X and Y axes all at a frequency of 0.5Hz.

This scenario compares the output of the force approximation control scheme when using the force input and its estimate.

Scenario 5 - Rendering a force in the vertical axis with uncompensated hysteresis: The force input and the desired force are the same as in scenario 3, however, the torque generated by the brake is subject to hysteresis. This scenario tests the ability of the observer to converge when the device model does not account for all device dynamics.

Scenario 6 - Rendering a varying force, with a varying force input and uncompensated hysteresis: The force input and the desired force are the same as in scenario 4, however, the torque generated by the brakes is subject to hysteresis. This scenario tests the performance of the NDO and force control scheme from [15] when the force input is not the only disturbance in the system.

The simulations are conducted using MATLAB Simulink 2020a running at 1kHz sampling frequency. The device dynamics obey the equations given in Sect. 2.1 but the gravity is omitted in the simulations such that the only force acting on the device is the force input of the user. The brake hysteresis in scenarios 5 and 6 is modelled using the Presiach hysteresis model described below.

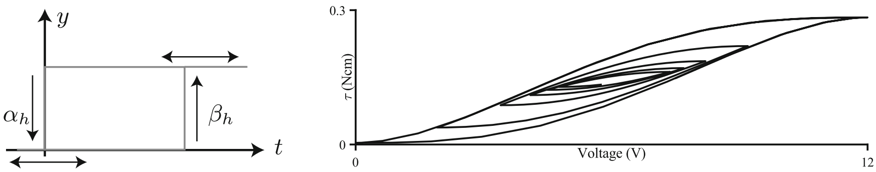

(b)

(a)

Fig. 3. (a) shows the hysteresis loop of a nonideal relay with excitation thresholds of α and β while (b) shows the hysteresis curve for the simulation imitates the curve of the actual particle brakes.

3.1 Hysteresis Model

The Preisach model is constructed using the model of a nonideal relay hysteron, see Fig. 3(a), with a square hysteresis loop described by α_h and β_h excitation thresholds such that,

$$y(t) = \begin{cases} 1 & \text{if } t \leq \alpha_h \\ y(t-1) & \text{if } \alpha_h < t < \beta_h \\ 0 & \text{if } t \geq \beta_h \end{cases} \tag{6}$$

where $y(t)$ is the output of the relay for input t, and $y(t-1)$ represents the previous output value. The model assumes that the magnetization properties of an object are a result of integrating the magnetization of many independent hysterons $\gamma_{\alpha_h,\beta_h}$ modelled in (6), such that

$$y(t) = \iint\limits_{\alpha_h \geq \beta_h} \mu(\alpha_h, \beta_h)\ \gamma_{\alpha_h,\beta_h}\ d\alpha_h\ d\beta_h \tag{7}$$

where $\mu(\alpha_h, \beta_h)$ is the Preisach density function [5,20]. The analytical solution to (7) does not exist and, thus, its implementation is discretized into a finite number of hysterons. The shape of the resulting hysteresis loop is defined by

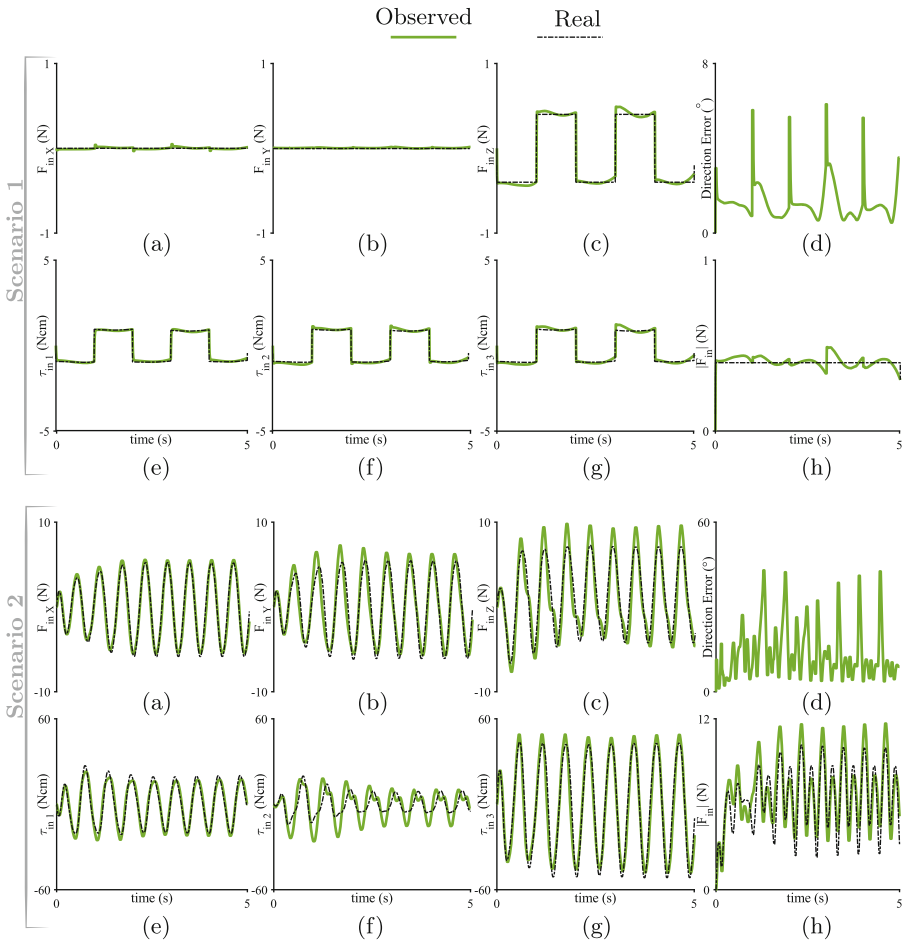

Fig. 4. The results for scenarios 1 and 2 where (a), (b), (c) show the forces input and its estimate in the X, Y, and Z axes, the torque inputs for the three joints are in (e), (f), (g). The angle between the actual force input and the estimate is shown in (d) and the magnitude difference in (h).

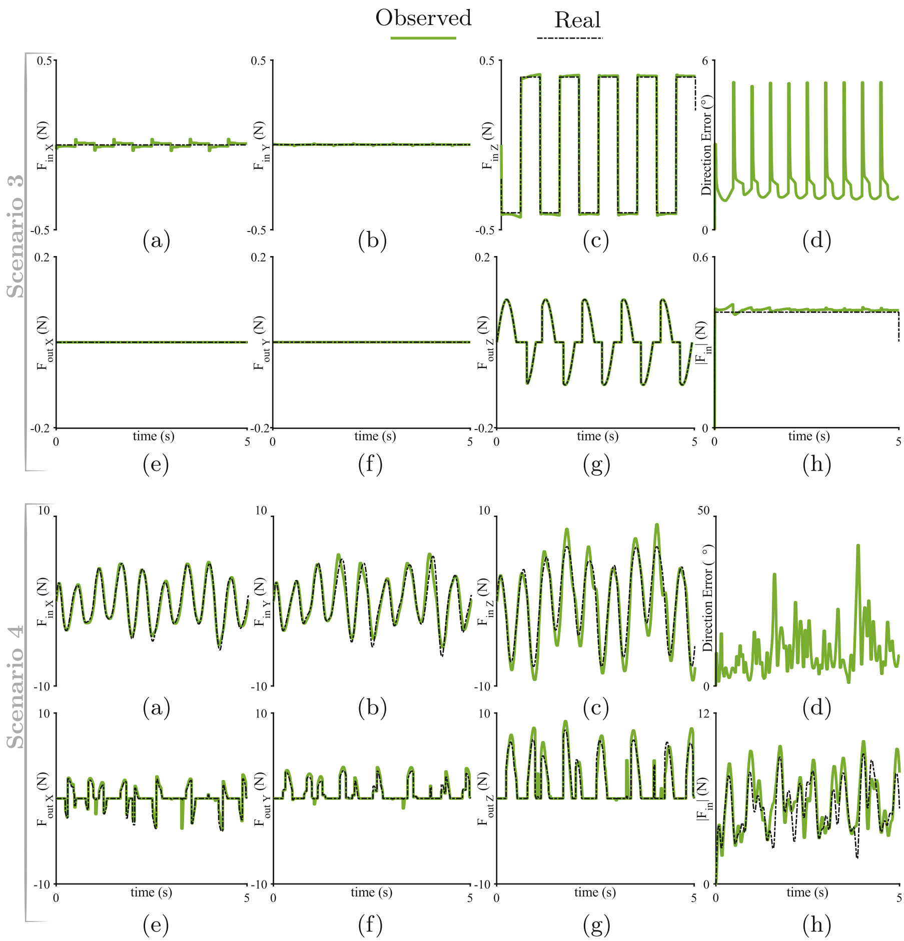

Fig. 5. The results for scenarios 3 and 4 where (a), (b), (c) show the forces input and its estimate in the X, Y, and Z axes and the force calculated by the controller using the actual and the estimated force input in the X, Y, and Z axes is shown in (e), (f), (g). The angle between the actual force input and the estimate force input is shown in (d) and the magnitude difference is given in (h).

the Preisach density function, however, finding such a function is difficult [20]. The Presach function is approximated as a matrix of coefficients created using a series of linear operations, thus obtained model results in the hysteresis loop shown in Fig. 3(b).

3.2 Results

The results for scenarios 1 and 2 are given in Fig. 4. Each set of results compares the force input and its estimate in the X, Y, and Z axes in (a), (b), (c), respec-

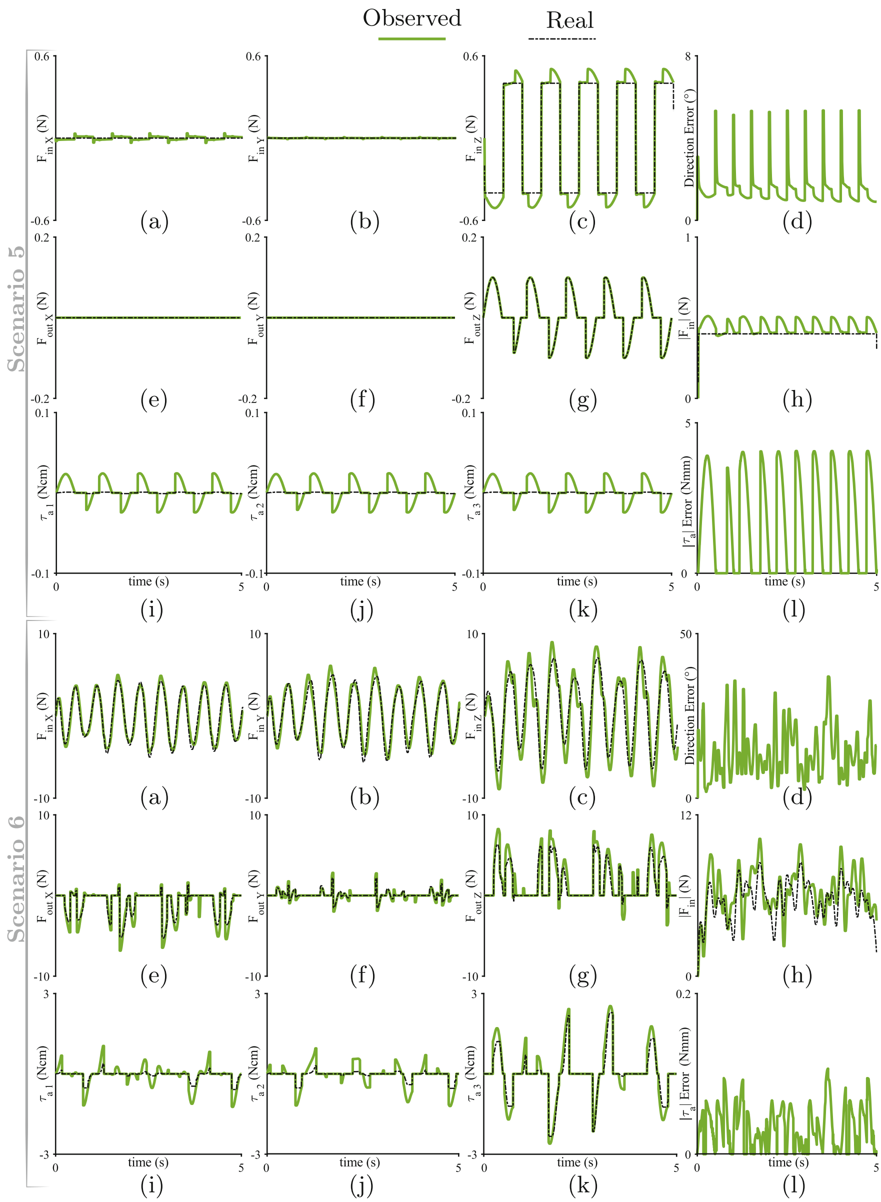

Fig. 6. The results for scenarios 5 and 6 where (a), (b), (c) show the force input and its estimate in the X, Y, and Z axes and the force calculated by the controller using the actual and estimated force input in the X, Y, and Z axes is shown in (e), (f), (g). The angle between the actual force input and the estimate is shown in (d) and the magnitude difference in (h). The effects of hysteresis on torque output of each brake is shown in (i), (j), and (k). Lastly, (l) shows the normalized error between the ideal applied torque and the actual applied torque.

tively. Subfigures (e), (f), (g), compare the actual torque input and its estimate at each of the three actuated joints. The angle between the actual force input and its estimate is shown in (d), while (h) compares their magnitudes.

Scenario 3 and 4 results are presented in Fig. 5. Subfigures (a), (b), and (c) show the force input and its estimate in the X, Y, and Z axes, respectively. The force calculated by the force approximation scheme using the force input and its estimates are compared in (e), (f), and (g), one for each of the spatial axes. The angle between the force input and its estimate is shown in (d), while (h) compares their magnitude.

Lastly, scenarios 5 and 6 are shown in Fig. 6, with (a), (b), (c) showing the force input and its estimate in the X, Y, and Z axes; (e), (f), (g) compare the output of the force approximation scheme using force input and its estimate; (i), (j), (k) compare desired torque and the hysteresis-uncompensated torque output of the brakes, while (l) shows the normalized error between the ideal and the actual torque applied to the brakes. The angle between the force input and its estimate is shown in (d). Finally (h) compares the actual and estimated force magnitudes. The mean and maximum direction error as well as the mean magnitude errors between the force input and its estimate are given in Table 3 for all six scenarios.

4 Discussion

First let us analyze the performance of the NDO in terms of force estimation, then discuss how errors in the force estimate affects the performance of the force approximation control scheme, and finish with the discussion of unmodelled hysteresis and its impact on the force estimation and control.

4.1 Force and Torque Estimation

In scenarios 1 and 2 the device is subjected only to the force input of the user. Ideally, there should be no difference between the input force and the resulting torque, and their estimates. In reality, however, the nonlinearity of the system

Table 3. The mean and maximum direction error along with the mean magnitude error between the force input and its estimate for the six scenarios.

Scenario	Mean direction error (deg)	Max direction error (deg)	mean magnitude error (%)
1	1.46	6.07	1.88
2	13.55	42.93	7.86
3	1.62	5.2	1.92
4	10.31	41.5	8.61
5	1.60	5.35	11.57
6	13.78	36.96	11.15

creates a discrepancy between the observer approximation and the torque inputs leading to a difference in both the magnitude and direction.

In the first scenario, a vertical force is applied to the end-effector, and since the device is in the centre of its workspace, that is $\theta_{11} = \theta_{12} = \theta_{13}$, the torque applied to each brake is the same. The results from Fig. 4 show that the estimated torques differ depending on the brake; the torque estimate at the first joint, shown in (e), is accurate while the estimates for joints two and three, see (f) and (g), exhibit some overshoot. This type of inaccuracy is intrinsic to the NDO as similar patterns can be seen in results obtained in [2,13]. These errors in the torque estimate translate to errors in the estimated force, as shown in (a), (b), and (c). From (d) and (f) it is evident that when the force input changes direction there is a delay in the response of the observer resulting in the angle and magnitude difference between the force input and its estimate. The direction error after the instantaneous change in the force direction is initially 6°, but it quickly converges to below 2°. The magnitude of the force also shows a large initial spike but likewise, it converges to approximately 2%. On average the direction error of the force estimate is 2° and the magnitude error is 1.5%. Note, however, that this is the worst-case scenario for the NDO as the disturbance is not a smooth function. Despite the unfavourable conditions the observer can still provide an accurate force estimate.

The force input in the second scenario is a smooth sinusoidal function acting in all three axes. The observer estimates the torque applied to each of the three joints with varying results. For instance, the estimate for the first and third joints, shown in Fig. 4(e) and (g), closely tracks the torque input, however, joint two, shown in (f), differs from the actual input torque. This error, however, does not seem to significantly affect the force estimate shown in (a), (b) and (c). Like in scenario 1, the error in the estimate is the greatest when the force direction changes rapidly, however, since the input is smooth the spikes in the direction error, shown in (d), and magnitude, shown in (h), are far less pronounced. The maximum direction error is 43° but on average the error is only 14° while the average magnitude error is about 8%.

4.2 Force Approximation Using Estimated Forces

Scenarios 3 and 4 incorporate the force approximation scheme from [15] and compares forces calculated by the controller using the input force measurement and its estimate. Ideally, the force output calculated by the controller based on the input force estimate should be the same as the one calculated using the actual force input. The results for scenarios 1 and 2, however, show that the estimated force may have a different direction and magnitude than the actual force. In scenario 3, the force input and the desired force act in the vertical direction and thus rendering the force does not require force approximation. On the other hand, in scenario 4 both the force input and the desired force act in all three directions meaning that there will be instances where force will need to be approximated.

Similar to the previous two scenarios, the observer estimates the force input with an average direction error of 2° and 10° for scenarios 3 and 4, respectively and an average magnitude error of 2% and 9%, respectively. The controller output using the true and estimated force input are similar for the two scenarios, as shown in Fig. 5(e), (f), and (g) for each of the three axes. Notably, the output based on the observed force input is higher when the force estimate is used. The cause of this anomaly is likely the overestimation of the force input magnitude which can be observed in (h). Such overestimation changes the balance of forces at the end-effector which may lead to stiction. The direction error, on the other hand, does not seem to have a major effect on the output of the controller.

4.3 Effects of Unmodelled Dynamics

Scenarios 5 and 6 test the sensitivity of the NDO to unmodelled dynamics, such as the brake hysteresis. Since the user is no longer the sole contributor of disturbance in the system the resulting force estimate is subjected to both the hysteresis and the user input.

The results in Fig. 6 (i), (j), and (k) show a significant difference between the output of the brake with and without unmodelled hysteresis. In both scenarios 5 and 6, the torque output by the brake is significantly smaller than the desired torque and the error is most pronounced when rending low torques, likely due to the highly nonlinear hysteresis loop.

The resulting force input estimate, shown in (a), (b), and (c), causes a noticeable increase in the error when compared with Fig. 5. In scenario 5 the error in the direction of the force input is nearly the same as in scenario 3, which is to be expected as the torque applied to each brake is equal. However, both the mean and the maximum magnitude errors in scenario 5, respectively 12% and 35%, are higher than what is observed in scenario 3, that is 2% and 6%. In scenario 6, on the other hand, the mean direction error is higher than in scenario 4, 14° compared with 10°. The magnitude error is also higher in scenario 6 compared with scenario 5, respectively 11% and 8%, which should increase the force output error of the controller.

In scenario 5 there is no difference in the output of the controller using the force input and its estimate, as shown in (e), (f), and (g). In scenario 6, on the other hand, the error in the force input estimate is noticeably higher than that in scenario 5. This indicates that unmodeled dynamics of the device can further promote stiction and, thus, must be compensated to guarantee the best performance. Despite the exaggerated effects of modelled hysteresis, the results clearly show that the NDO is versatile and it can provide an estimate of the force input.

5 Conclusions

Control schemes for passive haptic devices depend on force measurements and thus typically require force sensors. To reduce the reliance on the force sensor, we propose the use of a nonlinear disturbance observer (NDO) for sensorless force estimation. The proposed approach is tested using a dynamic simulation of the 3-DOF parallel passive device from [15]. The results show that the NDO can estimate the force input with a magnitude error lower than 9% and the direction error of 13° or less. The preliminary tests show that the force estimate obtained using the NDO can be used in force approximation control schemes as a replacement for a force sensor, though the concept requires further experimental validation.

It remains to be seen how unmodelled dynamics affect the force estimation in experimental tests. For large magnitudes of the input force, the disturbances caused by hysteresis, friction, and unmodeled dynamics become insignificant, meaning that the observed disturbance should closely match the user force input. On the other hand, when the force input is small these effects may dominate the response resulting in less accurate force approximation. An accurate Lagrangian model of the 3-DOF passive device proposed in [21] may improve accuracy at a cost of increasing computational cost [1,16]. Modelling particle brakes using Presiach model [20] or a more sophisticated approach like Boc-Wen Model [8] can further improve the accuracy of the NDO.

The NDO can only estimate forces when the device is in motion; if brakes stop moving the system is no longer observable. In situations where the brakes do not move, for instance, if the virtual environment imposes high viscous damping, a force measurement will still be required. The control of stationary brakes, however, requires only the measurement of the force input direction which can be estimated using low fidelity force sensors such as strain gauges placed directly on the links of the device. As a result, it may be possible to improve performance and reduce the cost of passive haptic devices, making them a more viable option in many haptic applications.

References

1. Briot, S., Khalil, W.: Dynamics of Parallel Robots. Springer, Cham (2015). https://doi.org/10.1007/978-3-319-19788-3
2. Chen, W.H., Ballance, D.J., Gawthrop, P.J., O'Reilly, J.: A nonlinear disturbance observer for robotic manipulators. IEEE Trans. Ind. Electron. **47**(4), 932–938 (2000)
3. Cho, C., Song, J.B., Kim, M.: Design and control of a planar haptic device with passive actuators based on passive force manipulability ellipsoid (FME) analysis. J. Robot. Syst. **22**(9), 475–486 (2005)
4. Cho, C., Song, J.B., Kim, M.: Energy-based control of a haptic device using brakes. IEEE Trans. Syst. Man Cybern. **37**(2), 341–349 (2007)
5. Diep, B.T., Vo, N., Le, T.D.: Hysteresis identification of bidirectional magneto-rheological actuators employing Preisach model. In: Applied Mechanics and Materials, vol. 889, pp. 355–360. Trans Tech Publ. (2019)
6. Flores-Mendez, J.D., Schiøler, H., Madsen, O., Bai, S.: Impedance control and force estimation of a redundant parallel kinematic manipulator. In: Gusikhin, O., Madani, K. (eds.) ICINCO 2017. LNEE, vol. 495, pp. 174–191. Springer, Cham (2020). https://doi.org/10.1007/978-3-030-11292-9_9

7. Gupta, A., O'Malley, M.K.: Disturbance-observer-based force estimation for haptic feedback. J. Dyn. Syst. Meas. Control **133**(1) (2011)
8. Ismail, M., Ikhouane, F., Rodellar, J.: The hysteresis Bouc-Wen model, a survey. Arch. Comput. Methods Eng. **16**(2), 161–188 (2009)
9. Karbasizadeh, N., Zarei, M., Aflakian, A., Masouleh, M.T., Kalhor, A.: Experimental dynamic identification and model feed-forward control of Novint Falcon haptic device. Mechatronics **51**, 19–30 (2018)
10. Katsura, S., Matsumoto, Y., Ohnishi, K.: Analysis and experimental validation of force bandwidth for force control. IEEE Trans. Ind. Electron. **53**(3), 922–928 (2006)
11. Komada, S., Nomura, K., Ishida, M., Hori, T.: Robust force control based on compensation for parameter variations of dynamic environment. IEEE Trans. Ind. Electron. **40**(1), 89–95 (1993)
12. Komada, S., Ohnishi, K.: Force feedback control of robot manipulator by the acceleration tracing orientation method. IEEE Trans. Ind. Electron. **37**(1), 6–12 (1990)
13. Korayem, M.H., Haghighi, R.: Nonlinear disturbance observer for robot manipulators in 3D space. In: Xiong, C., Huang, Y., Xiong, Y., Liu, H. (eds.) ICIRA 2008. LNCS (LNAI), vol. 5314, pp. 14–23. Springer, Heidelberg (2008). https://doi.org/10.1007/978-3-540-88513-9_3
14. Lacki, M., Rossa, C.: On the feasibility of multi-degree-of-freedom haptic devices using passive actuators. In: 2019 IEEE/RSJ International Conference on Intelligent Robots and Systems (IROS), pp. 7288–7293. IEEE (2019)
15. Łącki, M., Rossa, C.: Design and control of a 3 degree-of-freedom parallel passive haptic device. IEEE Trans. Haptics **13**(4), 720–732 (2020)
16. Merlet, J.P.: Parallel Robots, vol. 128, 2nd edn. Springer, Netherlands (2000). https://doi.org/10.1007/978-94-010-9587-7
17. Mohammadi, A., Marquez, H.J., Tavakoli, M.: Nonlinear disturbance observers: design and applications to Euler Lagrange systems. IEEE Control Syst. Mag. **37**(4), 50–72 (2017)
18. Murakami, T., Yu, F., Ohnishi, K.: Torque sensorless control in multidegree-of-freedom manipulator. IEEE Trans. Ind. Electron. **40**(2), 259–265 (1993)
19. Nikoobin, A., Haghighi, R.: Lyapunov-based nonlinear disturbance observer for serial n-link robot manipulators. J. Intell. Robot. Syst. **55**(2–3), 135–153 (2009)
20. Stakvik, J.Å., Ragazzon, M.R., Eielsen, A.A., Gravdahl, J.T.: On implementation of the Preisach model: Identification and inversion for hysteresis compensation. Model. Identif. Control: Nor. Res. Bull. **36**(3), 133–142 (2015). https://doi.org/10.4173/mic.2015.3.1
21. Stamper, R.E.: A three degree of freedom parallel manipulator with only translational degrees of freedom. Ph.D. thesis, University of Maryland (1997)